

## Article

# Synthesis of $Zn_3V_2O_8/rGO$ Nanocomposite for Photocatalytic Hydrogen Production

Fahad A. Alharthi <sup>\*</sup>, Alanood Sulaiman Ababtain , Hamdah S. Alanazi, Wedyan Saud Al-Nafaei and Imran Hasan <sup>\*</sup> 

Department of Chemistry, College of Science, King Saud University, Riyadh 11451, Saudi Arabia

<sup>\*</sup> Correspondence: fharthi@ksu.edu.sa (F.A.A.); iabdulateef@ksu.edu.sa (I.H.)

**Abstract:** In this study, zinc vanadate/reduced graphene oxide ( $Zn_3V_2O_8/rGO$ ) composite has been synthesized via a simple approach. Advanced characterization techniques (powder X-ray, scanning electron microscopy, energy dispersive X-ray spectroscopy and ultraviolet-visible (UV-vis) spectroscopy) have been used to authenticate the formation of  $Zn_3V_2O_8/rGO$  composite. Subsequently,  $Zn_3V_2O_8/rGO$  was applied as photo-catalyst for hydrogen generation using photo-catalysis. The  $Zn_3V_2O_8/rGO$  photo-catalyst exhibited a good hydrogen generation amount of  $104.6 \mu\text{molg}^{-1}$ . The  $Zn_3V_2O_8/rGO$  composite also demonstrates excellent cyclic stability which indicated better reusability of the photo-catalyst ( $Zn_3V_2O_8/rGO$ ). This work proposes a new photo-catalyst for  $H_2$  production application. We believe that the presence of synergistic interactions was responsible for the improved photo-catalytic properties of  $Zn_3V_2O_8/rGO$  composite. The  $Zn_3V_2O_8/rGO$  composite is an environmentally friendly and cost-effective photo-catalyst and can be used for photo-catalytic applications.

**Keywords:** zinc vanadate; hydrogen production;  $Zn_3V_2O_8/rGO$ ; photo-catalyst



**Citation:** Alharthi, F.A.; Ababtain, A.S.; Alanazi, H.S.; Al-Nafaei, W.S.; Hasan, I. Synthesis of  $Zn_3V_2O_8/rGO$  Nanocomposite for Photocatalytic Hydrogen Production. *Inorganics* **2023**, *11*, 93. <https://doi.org/10.3390/inorganics11030093>

Academic Editors: Alejandro Pérez-Larios and Oomman K. Varghese

Received: 23 December 2022

Revised: 26 January 2023

Accepted: 28 January 2023

Published: 24 February 2023



**Copyright:** © 2023 by the authors. Licensee MDPI, Basel, Switzerland. This article is an open access article distributed under the terms and conditions of the Creative Commons Attribution (CC BY) license (<https://creativecommons.org/licenses/by/4.0/>).

## 1. Introduction

Growing environmental degradation and a warming planet have an impact on life on earth and are serious issues for the present and the future [1–3]. A quick response or solution is needed to prevent impending crisis [1]. Researchers have discovered that the main cause of these problems, including the emission of greenhouse gases, is the over-use of fossil fuels for energy production [4–6]. Additionally, as fossil fuels are a key source of energy production today, their replacement with alternatives that are more efficient is crucial for both helping to reduce greenhouse gas emissions and ensuring enough energy supply [7].

Renewable energy sources such as wind and solar have severe limits due to low efficiency and high production costs [8]. Hydrogen may be an alternative energy source to overcome the energy crisis [9]. In recent years, hydrogen production has gained much attention because of its clean and efficient combustion [9]. Firstly, Fujishima and colleagues developed a  $TiO_2$  based electrode for hydrogen production application under UV illumination [10]. There are several reports available on photo-catalytic hydrogen evolution [11–13]. It is a challenging task to develop a highly efficient photo-catalyst for this [13]. The band gap of the photo-catalyst plays a significant role in the hydrogen evolution process [14]. In addition, morphological features of the photo-catalyst may also affect its performance in the hydrogen evolution process [15]. Surface area, mechanical stability and structural morphology may also play a significant role in photo-catalytic hydrogen production [15,16].

Nanostructured materials have the potential to separate electron-hole pairs and provide a better path for electron transportation [17]. Moreover, stability of the photo-catalyst is also an important factor for its potential application in large-scale hydrogen production [18]. Previous years have witnessed the fabrication of various novel catalysts such as

TiO<sub>2</sub>, C<sub>3</sub>N<sub>4</sub>, CdS, ZnO and MoS<sub>2</sub> for hydrogen evolution application [17–21]. It is still a challenge to design and develop a cost effective and eco-friendly photo-catalyst.

Recently, transition metal vanadates (TMVs) have drawn extensive attention for energy related applications (supercapacitor, batteries) due to their low cost, changeable oxidation state and availability [22–25]. A variety of TMV materials, including MV<sub>2</sub>O<sub>4</sub>, M<sub>3</sub>V<sub>2</sub>O<sub>8</sub>, MVO<sub>4</sub>, MV<sub>3</sub>O<sub>8</sub>, M<sub>2</sub>V<sub>2</sub>O<sub>7</sub> and MV<sub>2</sub>O<sub>6</sub> (M = Fe, Ni, Mn, Zn) have been utilized in various optoelectronic applications [24–32]. Vanadium-based photo-catalysts are attracting much interest for their photo-catalytic performance due to their band gap, potential, and stable chemical properties [33]. Kudo and colleagues used the BiVO<sub>4</sub> monoclinic electrode material for O<sub>2</sub> evolution under visible light irradiation [34]. BiVO<sub>4</sub> was utilized by Liu and colleagues for photo-reduction of CO<sub>2</sub> in water [35]. Li et al. reported photo-reduction of CO<sub>2</sub> into sustainable hydrocarbon fuel using Fe<sub>2</sub>VO<sub>4</sub> [36]. Ag<sub>3</sub>VO<sub>4</sub> was prepared using the solid state reaction technique and its effectiveness as a photo-catalyst to generate O<sub>2</sub> was evaluated by Konta et al. [37]. However, few reports are available on the use of TMVs as photo-catalyst for hydrogen production. Sekar et al. [38] reported the synthesis of BiVO<sub>4</sub>/graphene composite for hydrogen production and a hydrogen production rate of 11.5 μmol·g<sup>-1</sup>·h<sup>-1</sup>. Further, Dhabarde et al. [39] also reported on the facile conditions for the synthesis of BiVO<sub>4</sub>/graphene composite. This synthesized BiVO<sub>4</sub>/graphene composite was used as photo-catalyst towards hydrogen peroxide production [39]. This suggested that TMV based composite materials can be used as photo-catalyst in the hydrogen evolution process.

Zinc vanadium-based metal oxides, particularly Zn<sub>3</sub>V<sub>2</sub>O<sub>8</sub>, possess excellent optical properties and can be used as a photo-catalyst for hydrogen production application [30]. Zn<sub>3</sub>V<sub>2</sub>O<sub>8</sub> and its composite with rGO have been used in dye degradation and supercapacitor applications [27–29]. However, they have not been explored as photo-catalyst for hydrogen production applications.

In the present study, a novel photo-catalyst (Zn<sub>3</sub>V<sub>2</sub>O<sub>8</sub>/rGO) has been prepared for hydrogen production applications. So far, no report has been found on the use of Zn<sub>3</sub>V<sub>2</sub>O<sub>8</sub>/rGO as cost-effective photo-catalyst. According to our literature survey, this is the first report which demonstrated the use of Zn<sub>3</sub>V<sub>2</sub>O<sub>8</sub>/rGO as environmentally friendly and cost-effective photo-catalyst for photo-catalytic hydrogen production application.

## 2. Experimental Section

### 2.1. Materials and Chemicals

Chemicals and reagents, ammonium vanadate (99.95% trace metals, Merck, Rahway, NJ, USA), 2-methyl imidazole (99%, Merck), zinc nitrate hexahydrate (Fischer Scientific, Waltham, MA, USA), lactic acid (Fischer Scientific), ethanol (99.8%, Sigma, Kawasaki, Japan) and graphene oxide (powder, Merck) were used as received.

### 2.2. Apparatus

A Rigaku powder X-ray diffractometer was used for the powder X-ray diffraction (PXRD) study. Scanning electron microscopic (SEM) pictures of the samples were conducted on Zeiss microscope. The energy dispersive X-ray (EDS) study was carried out on a Horiba Instrument. Ultraviolet-visible (UV-vis) absorption spectra were recorded on an Agilent Cary Instrument. Photo-catalytic investigations were carried out using gas chromatograph.

### 2.3. Synthesis of Zn<sub>3</sub>V<sub>2</sub>O<sub>8</sub> and Zn<sub>3</sub>V<sub>2</sub>O<sub>8</sub>/rGO

The Zn<sub>3</sub>V<sub>2</sub>O<sub>8</sub> was obtained under facile conditions. As typical, 0.5 mmol of zinc nitrate hexahydrate and 0.33 mmol of ammonium vanadate were dissolved in 20 mL of distilled water and stirred for 30 min. Further, 4 mmol of 2-methyl imidazole was dissolved in distilled water and added to the above mixture and stirred for 5 min. The obtained precipitate was filtered, washed several times with water and ethanol and dried at 70 °C for 4 h and calcined at 450 °C for 3 h to obtain the Zn<sub>3</sub>V<sub>2</sub>O<sub>8</sub>. To obtain the Zn<sub>3</sub>V<sub>2</sub>O<sub>8</sub>/rGO composite, 50 mg of graphene oxide was dispersed in distilled water using

an ultra-sonicator for 1 h. Further,  $\text{Zn}_3\text{V}_2\text{O}_8$  was added to the graphene oxide dispersion and an appropriate amount of hydrazine hydrate was added to reduce the graphene oxide. The above mixture was sonicated for 2 h, filtered and washed and dried at  $70^\circ\text{C}$  for 4 h. The graphene oxide was purchased as reported elsewhere. The reduced graphene oxide was also prepared under similar conditions except for the addition of  $\text{Zn}_3\text{V}_2\text{O}_8$ .

#### 2.4. Photo-Catalytic Hydrogen Generation

For the photo-catalytic studies, an air-tight quartz tube was used as the photo-catalytic reactor system. First, 7 mL of lactic acid was poured in 100 mL of water. The photo-catalyst (50 mg;  $\text{Zn}_3\text{V}_2\text{O}_8$  or  $\text{Zn}_3\text{V}_2\text{O}_8/\text{rGO}$ ) was added to the prepared solution. Nitrogen ( $\text{N}_2$ ) gas was purged for 30 min to remove dissolved gases. Visible light source (300 W LED,  $\lambda = 420\text{ nm}$ ) was used for photo catalytic measurements. The generated  $\text{H}_2$  gas was collected at fixed time intervals and checked by gas chromatograph.

### 3. Results and Discussion

#### 3.1. Characterization

Phase purity of the prepared powder samples (rGO, GO,  $\text{Zn}_3\text{V}_2\text{O}_8$  and  $\text{Zn}_3\text{V}_2\text{O}_8/\text{rGO}$ ) was determined by using the powder X-ray diffraction (PXRD) technique (RINT:2500V X-ray diffractometer (Rigaku, Japan; Cu-K $\alpha$  irradiation and  $\lambda = 1.5406\text{ \AA}$ )). The PXRD diffractograms of the prepared GO and rGO samples were obtained at the 2Theta range of  $5\text{--}80^\circ$ . The PXRD pattern of GO exhibits the well-defined diffraction plane (001) of GO which indicated the formation of GO. In the case of rGO, a broad diffraction peak appeared which corresponded to the (002) diffraction plane of rGO and confirmed the successful conversion of GO to rGO (Figure 1a).

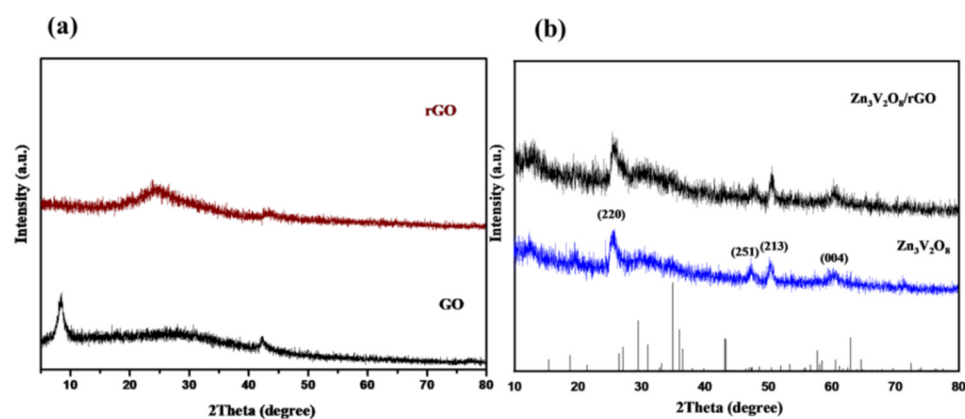


**Figure 1.** (a) PXRD patterns of GO and rGO (a). PXRD patterns of  $\text{Zn}_3\text{V}_2\text{O}_8$  and  $\text{Zn}_3\text{V}_2\text{O}_8/\text{rGO}$  (b).

The PXRD patterns of the  $\text{Zn}_3\text{V}_2\text{O}_8$  and  $\text{Zn}_3\text{V}_2\text{O}_8/\text{rGO}$  were also recorded at the 2Theta range of  $10\text{--}80^\circ$ . Figure 1b shows the PXRD patterns of the prepared  $\text{Zn}_3\text{V}_2\text{O}_8$  and  $\text{Zn}_3\text{V}_2\text{O}_8/\text{rGO}$ . The obtained PXRD results for  $\text{Zn}_3\text{V}_2\text{O}_8$  showed the presence of (220), (251), (213) and (004) diffraction planes of  $\text{Zn}_3\text{V}_2\text{O}_8$ . The PXRD pattern of  $\text{Zn}_3\text{V}_2\text{O}_8$  was well-matched with previous JCPDS no. 034-0378. No detected signal for (002) the diffraction plane in the PXRD pattern of  $\text{Zn}_3\text{V}_2\text{O}_8/\text{rGO}$  was attributed to the low content of rGO or poor crystalline nature of rGO. Previous studies also reported that rGO was visible in the PXRD data of the synthesized composite materials due to the poor crystalline nature of rGO and low rGO content [40]. Thus, it can be considered that  $\text{Zn}_3\text{V}_2\text{O}_8/\text{rGO}$  has been formed successfully.

Previous reports suggested that morphological features of the photo-catalyst play a vital role in photo-catalytic applications [41]. Thus, it is interesting to observe and study the top surface morphological properties of the prepared  $\text{Zn}_3\text{V}_2\text{O}_8$  and  $\text{Zn}_3\text{V}_2\text{O}_8/\text{rGO}$  composite. In this regard, scanning electron microscopy (SEM; Supra 55 Zeiss microscope; 10 keV) has been utilized to study the morphological properties of the different prepared

powder samples (rGO, GO,  $Zn_3V_2O_8$ , and  $Zn_3V_2O_8/rGO$ ). Figure 2a show the obtained SEM graph of GO. It is observed from the SEM investigations that GO consists of a sheet-like surface. Similarly, a SEM image of rGO is displayed in Figure 2b. The observations confirmed that rGO was comprised of a sheet-like surface which is the characteristic feature of rGO. The morphological characteristics of the  $Zn_3V_2O_8$  and  $Zn_3V_2O_8/rGO$  photo-catalysts were also studied. Figure 2c,d show the collected SEM graphs of the  $Zn_3V_2O_8$  photo-catalyst and suggest that  $Zn_3V_2O_8$  consists of an interconnected nanowire shaped surface morphology. The SEM graph of  $Zn_3V_2O_8/rGO$  was also collected at different magnifications. Figure 2e,f demonstrate the SEM graph of the  $Zn_3V_2O_8/rGO$  composite. According to the observations, it is clear that interconnected  $Zn_3V_2O_8$  nanowires have been grown on to the top surface of the rGO sheets. Although rGO could not be observed in the PXRD results, SEM images clearly show the presence of rGO sheets in the synthesized  $Zn_3V_2O_8/rGO$  composite. Thus, it is confirmed that  $Zn_3V_2O_8/rGO$  was synthesized successfully.

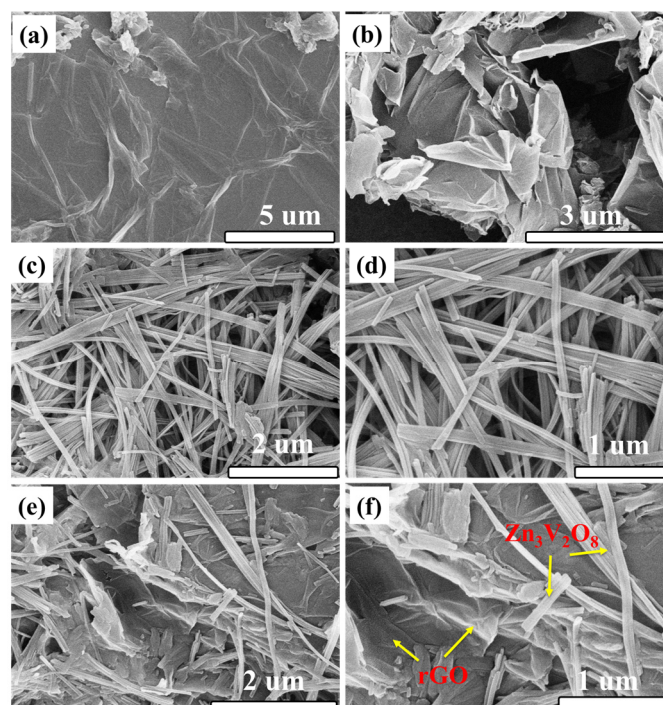


**Figure 2.** SEM image of GO (a), rGO (b),  $Zn_3V_2O_8$  (c,d) and  $Zn_3V_2O_8/rGO$  (e,f).

Energy-dispersive X-ray spectroscopy (EDS) plays a very important role in determining the elemental composition of the synthesized nanostructured materials. It is widely used as one of the important characterization tools for the determination of phase purity of the synthesized nanostructured materials. The EDS spectra of  $Zn_3V_2O_8$  and  $Zn_3V_2O_8/rGO$  composite were collected via an energy-dispersive X-ray spectroscope (Oxford Instruments X-max, Aztec, MA, USA). Figure 3a shows the EDS spectrum of the prepared  $Zn_3V_2O_8$  and obtained results show the signals for the presence of Zn, V and O elements. No other signal was detected, which indicated good phase purity of  $Zn_3V_2O_8$ . Figure 3b exhibits the EDS spectrum of  $Zn_3V_2O_8/rGO$  composite and shows the presence of signals for C, Zn, V and O elements. The presence of a signal for C element in the EDS spectrum authenticated the presence of rGO in the  $Zn_3V_2O_8/rGO$  composite. The band gap of the photo-catalyst is one of the most important features of the photo-catalytic hydrogen production process.

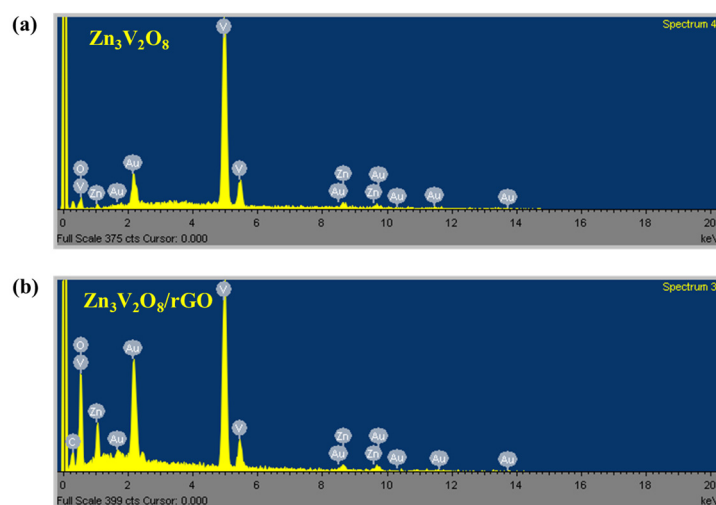


**Figure 3.** EDS spectrum of  $Zn_3V_2O_8$  (a) and  $Zn_3V_2O_8/rGO$  (b).

A suitable photo-catalyst should have narrow band gap with good stability. The optical band gap of the prepared  $Zn_3V_2O_8$  and  $Zn_3V_2O_8/rGO$  was also checked using ultraviolet-visible (UV-vis) absorption spectroscopy. Figure 4 demonstrated the UV-vis spectra of the prepared  $Zn_3V_2O_8$  and  $Zn_3V_2O_8/rGO$ . The band gaps of the  $Zn_3V_2O_8$  and  $Zn_3V_2O_8/rGO$  were calculated using Tauc-relation as given below,

$$\alpha h\nu = A (h\nu - E_g)^n \quad (1)$$

herein,  $\alpha$  is absorption coefficient,  $h$  = plank's constant,  $\nu$  is frequency,  $E_g$  = band gap energy, and  $n$  = transition value. The  $n = \frac{1}{2}$  has been taken for the direct band gap of  $Zn_3V_2O_8$  and  $Zn_3V_2O_8/rGO$ . The observation shows that  $Zn_3V_2O_8$  and  $Zn_3V_2O_8/rGO$  have band gaps of 3.5 eV (Figure S1) and 3.48 eV (Figure S2), respectively.

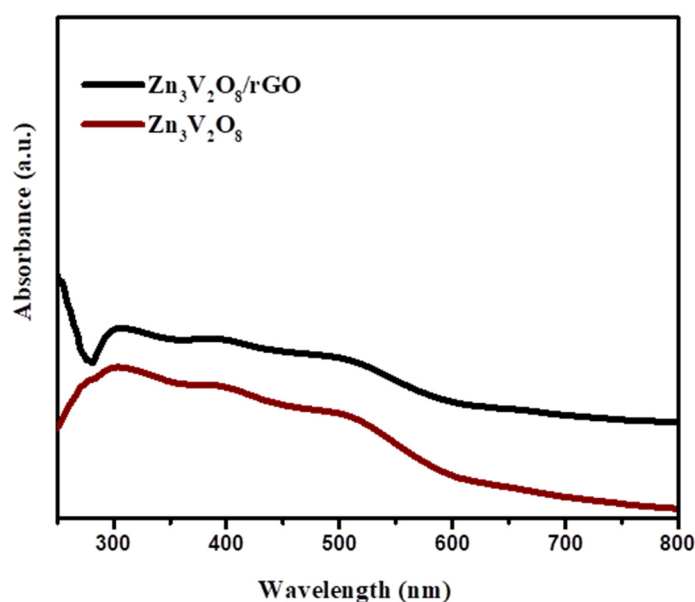


**Figure 4.** UV-vis spectra of  $Zn_3V_2O_8$  and  $Zn_3V_2O_8/rGO$ .

### 3.2. Hydrogen Generation

The hydrogen ( $H_2$ ) production studies were carried out with lactic acid in water solution in presence of photo-catalyst ( $Zn_3V_2O_8$  or  $Zn_3V_2O_8/rGO$ ). In the first step,  $N_2$  gas was passed into the prepared solution for 0.5 h. In previous studies [42], lactic acid

has been widely used as scavenger or sacrificial reagent for  $H_2$  production applications. Herein, we have adopted lactic acid for this purpose. Subsequently, this prepared solution was irradiated with LED lamp and after 1, 2, 3, 4, 5 and 6 h of light irradiations, the produced  $H_2$  was taken out from the quartz tube using a syringe and examined by gas chromatograph (TCD). Figure 5a demonstrates the photo-catalytic  $H_2$  generation amount using  $Zn_3V_2O_8$  as photo-catalyst under light irradiation and without light irradiation. The obtained  $H_2$  generation results indicated that no  $H_2$  was produced in the absence of light irradiation using  $Zn_3V_2O_8$  photo-catalyst. However, the  $Zn_3V_2O_8$  photo-catalyst exhibited the generation of  $24.56 \mu\text{mol}\cdot\text{g}^{-1}$   $H_2$ . It is obvious that  $Zn_3V_2O_8$  acted as an efficient photo-catalyst in presence of light irradiation only. In further investigations, the effect of light irradiation on  $H_2$  generation was also studied. The  $H_2$  generation was checked in the absence and presence of photo-catalyst ( $Zn_3V_2O_8$ ) under light irradiation. Figure 5b shows that  $24.56 \mu\text{mol}\cdot\text{g}^{-1}$   $H_2$  was produced in the presence of photo-catalyst ( $Zn_3V_2O_8$ ) under light irradiation whereas no  $H_2$  was generated in the absence of photo-catalyst ( $Zn_3V_2O_8$ ). This clearly indicates that the absence of photo-catalyst does not produce  $H_2$ . Furthermore, we have also employed  $Zn_3V_2O_8$ /rGO as photo-catalyst under similar conditions. The obtained results are summarized in Figure 5c.

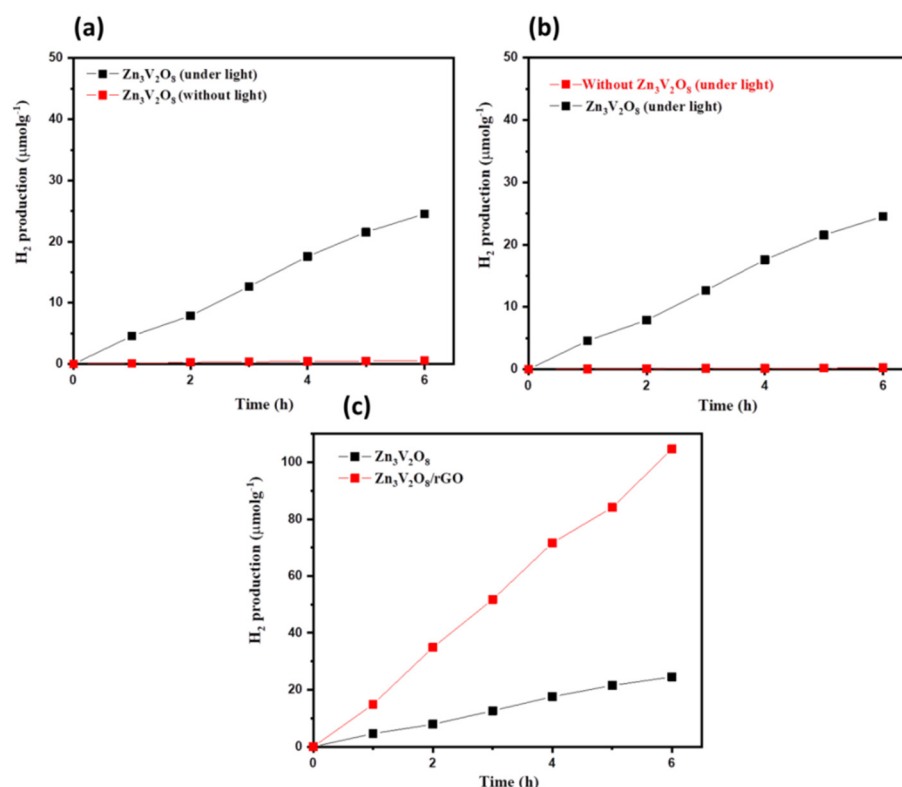


**Figure 5.** (a)  $H_2$  evolution study of  $Zn_3V_2O_8$  under light and without light. (b)  $H_2$  evolution study of with and without  $Zn_3V_2O_8$  under light and (c)  $H_2$  evolution study of  $Zn_3V_2O_8$  and  $Zn_3V_2O_8$ /rGO under light illuminations (c).

Figure 5c shows that improved  $H_2$  evolution was observed for  $Zn_3V_2O_8$ /rGO compared to  $Zn_3V_2O_8$ . This may be attributed to the excellent physiochemical properties of rGO and synergistic effects/interactions between  $Zn_3V_2O_8$  and rGO. The highest  $H_2$  generation amount of  $104.6 \mu\text{mol}\cdot\text{g}^{-1}$  was obtained using  $Zn_3V_2O_8$ /rGO photo-catalyst whereas  $Zn_3V_2O_8$  photo-catalyst produced a lower amount of  $24.56 \mu\text{mol}\cdot\text{g}^{-1}$ . From the photo-catalytic investigations, it can be clearly understood that  $Zn_3V_2O_8$ /rGO has excellent photo-catalytic behavior compared to  $Zn_3V_2O_8$ . In previous reports,  $\text{BiVO}_4$ /rGO was adopted as photo-catalyst for hydrogen evolution reaction and good photo-catalytic activity of  $0.75 \mu\text{mol}\cdot\text{h}^{-1}$  was reported [43].  $\text{BiVO}_4$  based photo-catalyst also exhibited

hydrogen production activity of  $195.6 \mu\text{mol}\cdot\text{h}^{-1}$  [44]. Another work also reported hydrogen production activity of  $0.92 \mu\text{mol}/\text{h}$  using carbon dot/ $\text{BiVO}_4$  quantum dot composite [45]. Quantum sized  $\text{BiVO}_4$  photo-catalyst showed decent hydrogen production activity [46]. Sekar et al. [38] have used  $\text{BiVO}_4$ , and  $\text{BiVO}_4/\text{rGO}$  as photo-catalyst for hydrogen generation.  $\text{BiVO}_4$  and  $\text{BiVO}_4/\text{rGO}$  exhibited hydrogen production activity of  $0.03$  and  $11.5 \mu\text{mol}\cdot\text{g}^{-1}\cdot\text{h}^{-1}$ , respectively [38]. The obtained hydrogen production activity in the present study is comparable with the previous reports as discussed above.

For practical purposes, the photo-catalyst should have excellent reusability. In this regard, reusability of the synthesized  $\text{Zn}_3\text{V}_2\text{O}_8/\text{rGO}$  photo-catalyst was investigated regarding photo-catalytic  $\text{H}_2$  generation. The obtained reusability results can be seen in Figure 6.

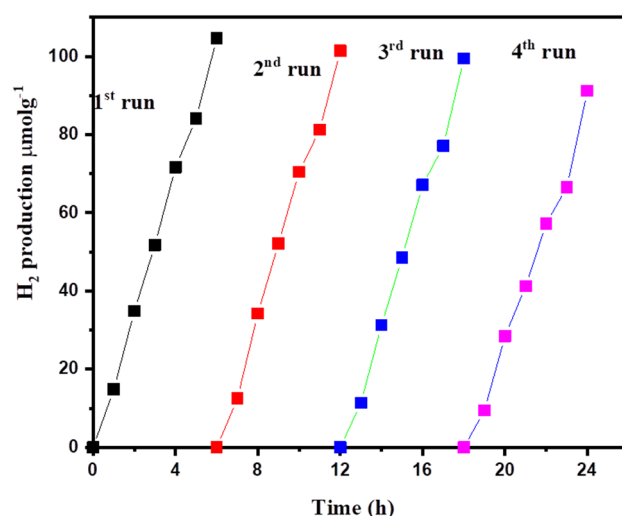
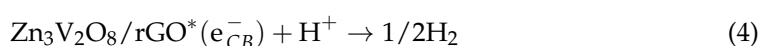
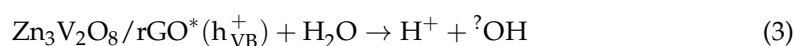
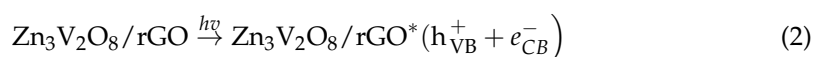
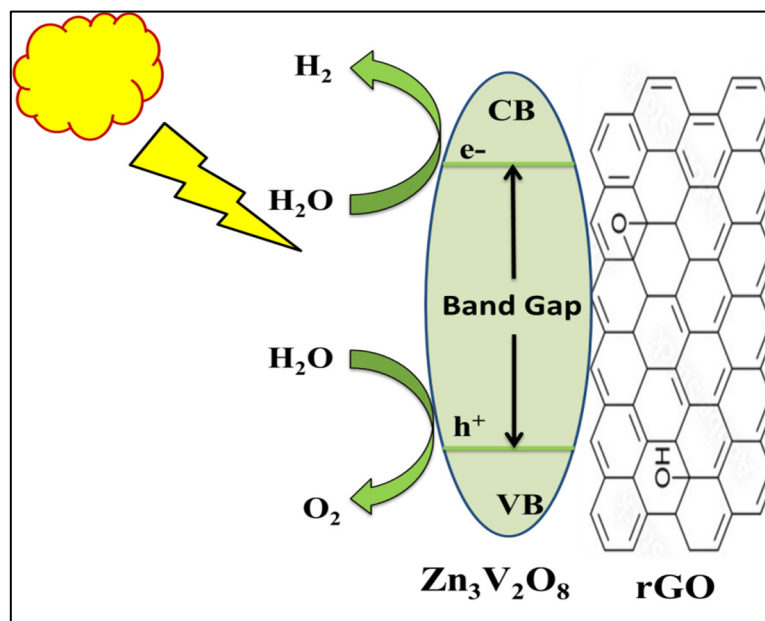


Figure 6. Reusability study of  $\text{Zn}_3\text{V}_2\text{O}_8/\text{rGO}$ .

The observations reveal that no significant changes were seen in  $\text{H}_2$  evolution after 4 cycles. This clearly suggested that  $\text{Zn}_3\text{V}_2\text{O}_8/\text{rGO}$  possess excellent cyclic stability up to 24 h with reusability up to four cycles. The SEM image of the  $\text{Zn}_3\text{V}_2\text{O}_8/\text{rGO}$  was also recorded after the reusability study. The SEM image is presented in Figure S3 which suggests good stability of the prepared  $\text{Zn}_3\text{V}_2\text{O}_8/\text{rGO}$ . The probable mechanism of  $\text{H}_2$  production has been illustrated in Scheme 1, occurring through water splitting and lactic acid reforming over the prepared  $\text{Zn}_3\text{V}_2\text{O}_8/\text{rGO}$  nanocomposite under light irradiation. The light irradiation of the material results in the generation of a photogenerated electron-hole pair (Equation (2)). The photogenerated electron can move from the conduction band (CB) of  $\text{Zn}_3\text{V}_2\text{O}_8$  to the CB of rGO and thereby it can be trapped due to the resonance effect. Thus, rGO with  $\text{Zn}_3\text{V}_2\text{O}_8$  assists in enhancing the separation between photogenerated electron and hole, thus improving the photocatalytic activity of the resulting material. The holes created at valence band (VB) react with surrounding water molecules to form  $\text{H}^+$  ions and reactive hydroxyl radicals ( $\cdot\text{OH}$ ) Equation (3). The  $\text{H}^+$  ions formed in VB move to CB and thereby interact with electrons on the surface of rGO and thus become reduced to  $\text{H}_2$  gas (Equation (4)). The lactic acid (sacrificial reagent) interacts with  $\cdot\text{OH}$  radicals and thus transforms into oxidized products and  $\text{H}^+$  ions (Equation (5)) which is further reduced to  $\text{H}_2$  gas on the rGO surface. Thus, both photocatalytic water splitting and the lactic acid reforming process contribute to hydrogen production synergistically [47,48].





**Scheme 1.** Schematic diagram shows the probable working mechanism for H<sub>2</sub> generation.

#### 4. Conclusions

In conclusion, a hybrid composite of zinc vanadate and reduced graphene oxide (Zn<sub>3</sub>V<sub>2</sub>O<sub>8</sub>/rGO) has been obtained using simple strategies. The fabricated Zn<sub>3</sub>V<sub>2</sub>O<sub>8</sub>/rGO composite possesses excellent photo-catalytic properties compared to Zn<sub>3</sub>V<sub>2</sub>O<sub>8</sub>. The Zn<sub>3</sub>V<sub>2</sub>O<sub>8</sub>/rGO composite exhibits a good hydrogen generation amount of 104.6 μmolg<sup>-1</sup>. Moreover, Zn<sub>3</sub>V<sub>2</sub>O<sub>8</sub>/rGO showed good cyclic stability up to 24 h, which suggested that Zn<sub>3</sub>V<sub>2</sub>O<sub>8</sub>/rGO has excellent reusability features. Although Zn<sub>3</sub>V<sub>2</sub>O<sub>8</sub>/rGO showed good photo-catalytic performance for H<sub>2</sub> production, its wide band gap of 3.48 eV limited its potential application for large scale production. The photo-catalytic properties of the Zn<sub>3</sub>V<sub>2</sub>O<sub>8</sub>/rGO can be further improved by incorporating unique and novel materials or methods. The Zn<sub>3</sub>V<sub>2</sub>O<sub>8</sub>/rGO photo-catalyst possesses good optical properties which suggests its further potential for waste water treatment, dye sensitized solar cells and photo-detector applications.

**Supplementary Materials:** The following supporting information can be downloaded at: <https://www.mdpi.com/article/10.3390/inorganics11030093/s1>. Figure S1. Tauc's plot of Zn<sub>3</sub>V<sub>2</sub>O<sub>8</sub>, Figure S2. Tauc's plot of Zn<sub>3</sub>V<sub>2</sub>O<sub>8</sub>/rGO, Figure S3. SEM image of Zn<sub>3</sub>V<sub>2</sub>O<sub>8</sub>/rGO after photocatalytic experiment

**Author Contributions:** Conceptualization, F.A.A.; Methodology, H.S.A. and I.H.; Software, H.S.A. and I.H.; Formal analysis, A.S.A. and W.S.A.-N.; Investigation, A.S.A. and W.S.A.-N.; Resources, A.S.A.; Data curation, I.H.; Writing—original draft, A.S.A.; Writing—review & editing, I.H.; Visualization, H.S.A. and I.H.; Supervision, F.A.A. and H.S.A.; Project administration, F.A.A.; Funding acquisition, F.A.A. All authors have read and agreed to the published version of the manuscript.

**Funding:** The authors extend their appreciation to the deputyship of Research and Innovation, Ministry of Education in Saudi Arabia for funding this research work through project number (IFK-SURG-2-1328).

**Data Availability Statement:** Data is contained in the manuscript and supporting information file.

**Acknowledgments:** The authors extend their appreciation to the deputyship of Research and Innovation, Ministry of Education in Saudi Arabia for funding this research work.

**Conflicts of Interest:** The authors declare no conflict of interest.

## References

1. Tao, X.; Zhao, Y.; Wang, S.; Li, C.; Li, R. Recent advances and perspectives for solar-driven water splitting using particulate photocatalysts. *Chem. Soc. Rev.* **2022**, *51*, 3561–3608. [[CrossRef](#)]
2. Ahmad, K.; Mobin, S. Organic-Inorganic Copper (II) Based Perovskites: A Benign Approach towards Low Toxic and Water Stable Light Absorbers for Photovoltaic Applications. *Energy Technol.* **2020**, *8*, 1901185. [[CrossRef](#)]
3. Ahmad, K.; Ansari, S.N.; Natarajan, K.; Mobin, S.M. A Two-Step Modified Deposition Method Based  $(\text{CH}_3\text{NH}_3)_3\text{Bi}_2\text{I}_9$  Perovskite: Lead Free, Highly Stable and Enhanced Photovoltaic Performance. *ChemElectroChem* **2019**, *6*, 1–6. [[CrossRef](#)]
4. Ahmad, K.; Mobin, S. Recent Progress and Challenges in  $\text{A}_3\text{Sb}_2\text{X}_9$ -Based Perovskite Solar Cells. *ACS Omega* **2020**, *5*, 28404–28412. [[CrossRef](#)] [[PubMed](#)]
5. Ma, D.; Shi, J.W.; Zou, Y.; Fan, Z.; Ji, X.; Niu, C. Highly Efficient Photocatalyst Based on a CdS Quantum Dots/ZnO Nanosheets 0D/2D Heterojunction for Hydrogen Evolution from Water Splitting. *ACS Appl. Mater. Interfaces* **2017**, *9*, 25377–25386. [[CrossRef](#)]
6. Chouhan, N.; Ameta, R.; Meena, R.K.; Mandawat, N.; Ghildiyal, R. Visible light harvesting Pt/CdS/Co-doped ZnO nanorods molecular device for hydrogen generation. *Int. J. Hydrogen Energy* **2016**, *41*, 2298–2306. [[CrossRef](#)]
7. Ma, D.; Shi, J.W.; Zou, Y.; Fan, Z.; Ji, X.; Niu, C.; Wang, L. Rational design of CdS@ZnO core-shell structure via atomic layer deposition for drastically enhanced photocatalytic  $\text{H}_2$  evolution with excellent photostability. *Nano Energy* **2017**, *39*, 183–191. [[CrossRef](#)]
8. Lv, J.X.; Zhang, Z.M.; Wang, J.; Lu, X.L.; Zhang, W.; Lu, T.B. In Situ Synthesis of CdS/Graphdiyne Heterojunction for Enhanced Photocatalytic Activity of Hydrogen Production. *ACS Appl. Mater. Interfaces* **2019**, *11*, 2655–2661. [[CrossRef](#)]
9. Vaishnav, J.K.; Arbuj, S.S.; Rane, S.B.; Amalnerkar, D.P. One dimensional CdS/ZnO nanocomposites: An efficient photocatalyst for hydrogen generation. *RSC Adv.* **2014**, *4*, 47637–47642. [[CrossRef](#)]
10. Fujishima, A.; Honda, K. Electrochemical Photolysis of Water at a Semiconductor Electrode. *Nature* **1972**, *238*, 37–38. [[CrossRef](#)]
11. Lingampalli, S.R.; Gautam, U.K.; Rao, C.N.R. Highly efficient photocatalytic hydrogen generation by solution-processed ZnO/Pt/CdS, ZnO/Pt/ $\text{Cd}_{1-x}\text{Zn}_x\text{S}$  and ZnO/Pt/ $\text{CdS}_{1-x}\text{Se}_x$  hybrid nanostructures. *Energy Environ. Sci.* **2013**, *6*, 3589–3594. [[CrossRef](#)]
12. Yang, G.R.; Yan, W.; Zhang, Q.; Shen, S.H.; Ding, S.J. One-dimensional CdS/ZnO core/shell nanofibers via single-spinneret electrospinning: Tunable morphology and efficient photocatalytic hydrogen production. *Nanoscale* **2013**, *5*, 12432–12439. [[CrossRef](#)] [[PubMed](#)]
13. Zhou, P.; Yu, J.G.; Jaroniec, M. All-Solid-State Z-Scheme Photocatalytic Systems. *Adv. Mater.* **2014**, *26*, 4920–4935. [[CrossRef](#)] [[PubMed](#)]
14. Lia, G.; Lian, Z.; Wang, W.; Zhang, D.; Li, H. Nanotube-confinement induced size-controllable  $\text{g-C}_3\text{N}_4$  quantum dots modified single-crystalline  $\text{TiO}_2$  nanotube arrays for stable synergetic photoelectrocatalysis. *Nano Energy* **2016**, *19*, 446–454. [[CrossRef](#)]
15. Jin, J.; Wang, C.; Ren, X.N.; Huang, S.Z.; Wu, M.; Chen, L.H.; Hasan, T.; Wang, B.J.; Li, Y.; Su, B.L. Anchoring ultrafine metallic and oxidized Pt nanoclusters on yolk-shell  $\text{TiO}_2$  for unprecedentedly high photocatalytic hydrogen production. *Nano Energy* **2017**, *38*, 118–126. [[CrossRef](#)]
16. Moa, H.; Song, C.; Zhou, Y.; Zhang, B.; Wang, D. Design and synthesis of porous Ag/ZnO nanosheets assemblies as super photocatalysts for enhanced visible-light degradation of 4-nitrophenol and hydrogen evolution. *Appl. Catal. B* **2018**, *221*, 565–573. [[CrossRef](#)]
17. Wang, X.; Li, Q.; Shi, P.; Fan, J.; Min, Y.; Xu, Q. Nickel Nitride Particles Supported on 2D Activated Graphene–Black Phosphorus Heterostructure: An Efficient Electrocatalyst for the Oxygen Evolution Reaction. *Small* **2019**, *15*, 1901530. [[CrossRef](#)]
18. Liu, W.; Wang, X.; Yu, H.; Yu, J. Direct Photoinduced Synthesis of Amorphous  $\text{CoMoS}_x$  Cocatalyst and Its Improved Photocatalytic  $\text{H}_2$ -Evolution Activity of CdS. *ACS Sustain. Chem. Eng.* **2018**, *6*, 12436–12445. [[CrossRef](#)]
19. Gong, S.; Jiang, Z.; Shi, P.; Fan, J.; Xu, Q.; Min, Y. Noble-metal-free heterostructure for efficient hydrogen evolution in visible region: Molybdenum nitride/ultrathin graphitic carbon nitride. *Appl. Catal. B* **2018**, *238*, 318–327. [[CrossRef](#)]
20. Wu, T.; Ma, Y.; Qu, Z.; Fan, J.; Li, Q.; Shi, P.; Xu, Q.; Min, Y. Black Phosphorus–Graphene Heterostructure-Supported Pd Nanoparticles with Superior Activity and Stability for Ethanol Electro-oxidation. *ACS Appl. Mater. Interfaces* **2019**, *11*, 5136–5145. [[CrossRef](#)]
21. Liao, K.; Chen, S.; Wei, H.; Fan, J.; Xu, Q.; Min, Y. Micropores of pure nanographite spheres for long cycle life and high-rate lithium–sulfur batteries. *J. Mater. Chem. A* **2018**, *6*, 23062–23070. [[CrossRef](#)]
22. Xing, M.; Kong, L.-B.; Liu, M.-C.; Liu, L.-Y.; Kang, L.; Luo, Y.-C. Cobalt vanadate as highly active, stable, noble metal-free oxygen evolution electrocatalyst. *J. Mater. Chem. A* **2014**, *2*, 18435–18443. [[CrossRef](#)]
23. Xiao, L.; Zhao, Y.; Yin, J.; Zhang, L. Clewlike  $\text{ZnV}_2\text{O}_4$  hollow spheres: Nonaqueous sol–gel synthesis, formation mechanism, and lithium storage properties. *Chem. Eur. J.* **2009**, *15*, 9442–9450. [[CrossRef](#)]
24. Zhang, Y.; Liu, Y.; Chen, J.; Guo, Q.; Wang, T.; Pang, H. Cobalt vanadium oxide thin nanoplates: Primary electrochemical capacitor application. *Sci. Rep.* **2014**, *4*, 5687. [[CrossRef](#)]
25. Ma, H.; Zhang, S.; Ji, W.; Tao, Z.; Chen, J. A- $\text{CuV}_2\text{O}_6$  nanowires: Hydrothermal synthesis and primary lithium battery application. *J. Am. Chem. Soc.* **2008**, *130*, 5361–5367. [[CrossRef](#)]
26. Butt, F.; Cao, C.; Ahmed, R.; Khan, W.; Cao, T.; Bidin, N.; Li, P.; Wan, Q.; Qu, X.; Tahir, M.; et al. Synthesis of novel  $\text{ZnV}_2\text{O}_4$  spinel oxide nanosheets and their hydrogen storage properties. *CrystEngComm* **2014**, *16*, 894–899. [[CrossRef](#)]

27. Shi, R.; Wang, Y.; Zhou, F.; Zhu, Y.  $\text{Zn}_3\text{V}_2\text{O}_7(\text{OH})_2(\text{H}_2\text{O})_2$  and  $\text{Zn}_3\text{V}_2\text{O}_8$  nanostructures: Controlled fabrication and photocatalytic performance. *J. Mater. Chem.* **2011**, *21*, 6313–6320. [[CrossRef](#)]
28. Mondal, C.; Ganguly, M.; Sinha, A.; Pal, J.; Sahoo, R.; Pal, T. Robust cubooctahedron  $\text{Zn}_3\text{V}_2\text{O}_8$  in gram quantity: A material for photocatalytic dye degradation in water. *CrystEngComm* **2013**, *15*, 6745–6751. [[CrossRef](#)]
29. Vijayakumar, S.; Lee, S.; Ryu, K. Synthesis of  $\text{Zn}_3\text{V}_2\text{O}_8$  nanoplatelets for lithium-ion battery and supercapacitor applications. *RSC Adv.* **2015**, *5*, 91822–91828. [[CrossRef](#)]
30. Sambandam, B.; Soundharajan, V.; Song, J.; Kim, S.; Jo, J.; Pham, D.T.; Kim, S.; Mathew, V.; Kim, J.  $\text{Zn}_3\text{V}_2\text{O}_8$  porous morphology derived through a facile and green approach as an excellent anode for high-energy lithium ion batteries. *Chem. Eng. J.* **2017**, *328*, 454–463. [[CrossRef](#)]
31. Xin, S.; Guo, Y.-G.; Wan, L.-J. Nanocarbon networks for advanced rechargeable lithium batteries. *Acc. Chem. Res.* **2012**, *45*, 1759–1769. [[CrossRef](#)] [[PubMed](#)]
32. Yao, X.; Kong, J.; Zhou, D.; Zhao, C.; Zhou, R.; Lu, X. Mixed transition-metal oxides: Design, synthesis, and energy-related applications. *Carbon* **2014**, *79*, 493–499. [[CrossRef](#)]
33. Ye, J.; Zou, Z.; Arakaw, H.; Oshikiri, M.; Shimoda, M.; Matsushita, A.; Shishido, T. Correlation of crystal and electronic structures with photophysical properties of water splitting photocatalysts  $\text{InMO}_4$  ( $M = \text{V}^{5+}, \text{Nb}^{5+}, \text{Ta}^{5+}$ ). *J. Photochem. Photobiol. A* **2002**, *148*, 79–83. [[CrossRef](#)]
34. Kudo, A.; Omori, K.; Kato, H. A Novel Aqueous Process for Preparation of Crystal Form-Controlled and Highly Crystalline  $\text{BiVO}_4$  Powder from Layered Vanadates at Room Temperature and Its Photocatalytic and Photophysical Properties. *J. Am. Chem. Soc.* **1999**, *121*, 11459–11467. [[CrossRef](#)]
35. Liu, Y.; Huang, B.; Dai, Y.; Zhang, X.; Qin, X.; Jiang, M.; Whangbo, M.-H. Selective Ethanol Formation from Photocatalytic Reduction of Carbon-dioxide in Water with  $\text{BiVO}_4$  Photocatalyst. *Catal. Commun.* **2009**, *11*, 210–213. [[CrossRef](#)]
36. Li, P.; Zhou, Y.; Tu, W.; Liu, Q.; Yan, S.; Zou, Z. Direct Growth of  $\text{Fe}_2\text{V}_4\text{O}_{13}$  Nanoribbons on a Stainless-Steel Mesh for Visible-Light Photoreduction of  $\text{CO}_2$  into Renewable Hydrocarbon Fuel and Degradation of Gaseous Isopropyl Alcohol. *ChemPlusChem* **2013**, *78*, 274–278. [[CrossRef](#)]
37. Konta, R.; Kato, H.; Kobayashi, H.; Kudo, A. Photophysical properties and photocatalytic activities under visible light irradiation of silver vanadates. *Phys. Chem. Chem. Phys.* **2003**, *5*, 3061–3065. [[CrossRef](#)]
38. Sekar, K.; Kassam, A.; Bai, Y.; Coulson, B.; Li, W.; Douthwaite, R.E.; Sasaki, K.; Lee, A.F. Hierarchical bismuth vanadate/reduced graphene oxide composite photocatalyst for hydrogen evolution and bisphenol A degradation. *Appl. Mater. Today* **2021**, *22*, 100963. [[CrossRef](#)]
39. Dhabarde, N.; Carrillo-Ceja, O.; Tian, S.; Xiong, G.; Raja, K.; Subramanian, V. Bismuth Vanadate Encapsulated with Reduced Graphene Oxide: A Nanocomposite for Optimized Photocatalytic Hydrogen Peroxide Generation. *J. Phys. Chem. C* **2021**, *125*, 23669–23679. [[CrossRef](#)]
40. Ahmad, K.; Mohammad, A.; Mathur, P.; Mobin, S.M. Preparation of  $\text{SrTiO}_3$  perovskite decorated rGO and electrochemical detection of nitroaromatics. *Electrochim. Acta* **2016**, *215*, 435–446. [[CrossRef](#)]
41. Chen, X.; Shen, S.; Guo, L.; Mao, S.S. Semiconductor-based Photocatalytic Hydrogen Generation. *Chem. Rev.* **2010**, *110*, 6503–6570. [[CrossRef](#)] [[PubMed](#)]
42. Yu, J.; Yu, Y.; Cheng, B. Enhanced visible-light photocatalytic  $\text{H}_2$ -production performance of multi-armed CdS nanorods. *RSC Adv.* **2012**, *2*, 11829–11835. [[CrossRef](#)]
43. Ng, Y.; Iwase, A.; Kudo, A.; Amal, R. Reducing Graphene Oxide on a Visible-Light  $\text{BiVO}_4$  Photocatalyst for an Enhanced Photoelectrochemical Water Splitting. *J. Phys. Chem. Lett.* **2010**, *17*, 2607–2612. [[CrossRef](#)]
44. Nagabhushana, G.P.; Nagaraju, G.; Chandrappa, G.T. Synthesis of bismuth vanadate: Its application in  $\text{H}_2$  evolution and sunlight-driven photodegradation. *J. Mater. Chem. A* **2013**, *1*, 388–394. [[CrossRef](#)]
45. Wu, X.; Zhao, J.; Guo, S.; Wang, L.; Shi, W.; Huang, H.; Liu, Y.; Kang, Z. Carbon dot and  $\text{BiVO}_4$  quantum dot composites for overall water splitting via a two-electron pathway. *Nanoscale* **2016**, *8*, 17314–17321. [[CrossRef](#)]
46. Sun, S.; Wang, W.; Li, D.; Zhang, L.; Jiang, D. Solar Light Driven Pure Water Splitting on Quantum Sized  $\text{BiVO}_4$  without any Cocatalyst. *ACS Catal.* **2014**, *4*, 3498–3503. [[CrossRef](#)]
47. Kondarides, D.I.; Daskalaki, V.M.; Patsoura, A.; Verykios, X.E. Hydrogen Production by Photo-Induced Reforming of Biomass Components and Derivatives at Ambient Conditions. *Catal Lett.* **2008**, *122*, 26–32. [[CrossRef](#)]
48. Wang, Y.; Liu, T.; Tian, W.; Zhang, Y.; Shan, P.; Chen, Y.; Wei, W.; Yuan, H.; Cui, H. Mechanism for Hydrogen Evolution from Water Splitting Based on a  $\text{MoS}_2/\text{WSe}_2$  Heterojunction Photocatalyst: A First-Principle Study. *RSC Adv.* **2020**, *10*, 41127–41136. [[CrossRef](#)]

**Disclaimer/Publisher's Note:** The statements, opinions and data contained in all publications are solely those of the individual author(s) and contributor(s) and not of MDPI and/or the editor(s). MDPI and/or the editor(s) disclaim responsibility for any injury to people or property resulting from any ideas, methods, instructions or products referred to in the content.